Soft Matter

Illumination-induced motion of a Janus nanoparticle in binary solvents

Journal:	*Soft Matter*
Manuscript ID	SM-ART-03-2019-000509.R1
Article Type:	Paper
Date Submitted by the Author:	21-May-2019
Complete List of Authors:	Araki, Takeaki; Kyoto University, Department of Physics Maciolek, Anna; Institute of Physical Chemistry, Polish Academy of Sciences, Soft Matter; Max-Planck-Institu fur Inteligente Systeme, Theory of Inhomogenous Condensed Matter

Journal Name

ARTICLE TYPE

Cite this: DOI: 10.1039/xxxxxxxxxx

Illumination-induced motion of a Janus nanoparticle in binary solvents†

Takeaki Araki,[a] and Anna Maciołek,[b,c]

Received Date
Accepted Date

DOI: 10.1039/xxxxxxxxxx

www.rsc.org/journalname

Using a fluid particle dynamics method we numerically investigate motion of a spherical Janus particle suspended in a binary liquid mixture, which emerge under heating of one-half of a colloid surface. The method treats simultaneously the flow of the solvent and the motion of the particle, hence, the velocity of the particle can be computed directly. Our approach accounts for a phenomenon of critical adsorption, therefore, a particle that is adsorptionwise nonneutral is always completely covered by an adsorption layer (droplet). In order to establish the mechanism of self-propulsion, we study systematically various combinations of adsorption preference on both hemispheres of the Janus colloid as function of the heating power for symmetric and nonsymmetric binary solvent and for various particle sizes in three spatial dimensions. Only for a particle, which heated hemisphere is neutral whereas the other hemisphere prefers one of the two components of the mixture, the reversal of the direction of motion occurs. The particle self-propels much faster in the nonsymmetric binary solvents. Self-propulsion originates from a gradient of mechanical stress, in a way similar to the Marangoni effect. This stress is not localized at the edge but distributed within the whole droplet. We compare our findings with the experimental observations and other theoretical results.

Introduction

Colloidal particles which self-propel when illuminated by light were developed to mimic an active motion observed in biology, e.g., swimming of a bacteria [1–4]. An interesting realization of such colloidal "artificial swimmer" was proposed by Bechinger and co-workers [5]. It involves a micron-sized Janus particles half-coated by a nano-thick gold [5] or carbon [6] cap and suspended in a mixed phase of a binary liquid solvent. Experiments demonstrated that the spherical Janus particle moves under illumination with green light of intensities lower than $\approx 10\ \mu W/\mu m^2$ in a way characteristic of the so called active Brownian motion [7], which is ballistic at short times and diffusive with an enhanced diffusion coefficient at long times [5,6].

This kind of light activated self-propellers proved to be very useful for exploring various aspects of active motion. This includes possibilities to control active motion both in time and in space, e.g., by employing spatial and temporal illumination patterns [6], the behavior in complex environments [5], or development of external control strategies to navigate light-activated colloids towards a target [8]. The latter aspect is important for application perspectives as micron-sized carriers for the delivery of drugs or as active building blocks for the assembly of microstructures. Further studies include motion in static light gradients [9,10] and in viscoelastic fluids [11,12], as well as the properties of asymmetric self-propelled objects and their motion in a gravitation field [13,14]. More recent research activities concern collective behavior such as clustering, which occurs in dense suspensions of self-propelling Janus colloids [15] or in a mixture of passive and active particles [16], and self-organisation of active particles [17].

Surprisingly, self-propulsion mechanism of this very successful class of artificial microswimmer is not yet understood in a full detail. Evidence has been gathered that the onset of the motion as well as its direction and speed depend sensitively on system parameters, such as wetting properties of both hemispheres of the Janus particle, the intensity of illumination, or the particle size. In their original paper, Bechinger an co-workers [5] trace the origin of the active motion to the local demixing of a binary solvent observed around the Janus colloid after illumination by light of sufficient intensity. It was argued that the golden cap, which strongly absorbs green light, is heated above the lower critical temperature T_c of the solvent and that resulting spinodal decomposition generates gradient of concentration that varies along the surface of the Janus particle. Therefore, in analogy with the catalytic active colloid [18–20], self-diffusiophoresis was initially suggested as the

[a]Department of Physics, Kyoto University, Kyoto 606-8502, Japan. E-mail: araki@scphys.kyoto-u.ac.jp
[b] Institute of Physical Chemistry, Polish Academy of Sciences, Kasprzaka 44/52, PL-01-224 Warsaw, Poland. E-mail: amaciolek@ichf.edu.pl
[c] Max-Planck-Institut für Intelligente Systeme, Heisenbergstr. 3, D-70569 Stuttgart, Germany.

plausible mechanism of particle motion. Self-thermophoresis was ruled out because in pure water no directed motion was observed at the similar illumination intensities.

According to the standard theory of phoresis [20–22], the colloid transport occurs due to processes occurring within solid/fluid interface at the surface of the particle. A nonuniform concentration around the particle gives rise, within the interface layer, to the unbalance pressure gradient along the surface of the particle. This in turn generates shear stress within the interface layer and, therefore, hydrodynamic flow of the solvent along the surface of the particle, which entails motion of the colloid. For the interfacial layer which is thin compared to the particle size, the flow is characterized by an effective slip velocity. The velocity of the particle follows from the requirement that hydrodynamic flow around the particle exerts no force and torque on it. Using this procedure, in Ref. [23] the self-propulsion velocity of the Janus particle was determined as a function of wetting properties of the two hemispheres and the surface temperature, which is related to the intensity of illumination. It was found that if the surface temperature exceeds T_c slightly or moderately, for all combinations of the wetting properties of the two hemispheres the particle moves towards the cap. When the two hemispheres prefer different components of the binary solvent, the velocity of the particle can change its sign provided the surface temperature is sufficiently high and the preferential adsorption of uncapped hemisphere is stronger. These predictions contradict experimental observations made for weakly hydrophilic silica particles capped with the hydrophilic-functionalized gold, which move away from the cap in the water-2,6 lutidine mixture for all studied values of illumination intensity [5,6,15].

Concerning possible combinations of hydrophilic/hydrophobic and heated/unheated hemispheres, the only other variant studied experimentally is that of weakly hydrophilic-hydrophobic Janus particle with hydrophobic hemisphere being heated. This includes a silica particle with the hydrophobic-functionalized cap in a water-2,6 lutidine mixture [5,6,15] and a silica particle with a hydrophobic carbon cap in a water-propylene glycol n-propyl ether (PnP) mixture [10]. Interestingly, the two realizations of the same type of Janus particle propel in the opposite direction. In the range of light intensities in which the propulsion velocity increases linearly with the applied intensity, the silica particle with hydrophobic golden cap moves towards the cap (which is consistent with diffusiophoresis), whereas the silica particle with the hydrophobic carbon cap moves away from the cap. This is very surprising, because one would expect the same mechanism of propulsion for the same type of the Janus particle. This fact has not been commented by the authors of these experiments [10].

Another intriguing experimental observation [10] concerns the behavior of silica particles with the carbon cap upon increasing the intensity of illumination beyond the linear regime. At a certain value of light intensity, which is higher for smaller colloids, one can see a sharp reversal of the direction of motion. Upon further increase of light intensity, the Janus particle stops self-propelling. These experimental findings were compared to numerical results from hydrodynamic description which, contrary to diffusiophoresis, assumes no slip velocity on the particle surface [10,24]. The observed rich variation of propulsion velocity as a function of illumination intensity was related to changes in the size and shape of the droplet (or two droplets) nucleated within a region enclosed by a temperature contour of T_c around the colloid.

The model employed in Refs. [10,24], referred to as diffuse interface approach, is a noiseless model H of critical dynamics of binary mixture [25], in which the preference of hemispheres of the Janus particle for a one component of the binary solvent (PnP) is accounted for via the wetting boundary conditions (BCs). These BCs ensure that the PnP droplet meets the surface at the prescribed microscale contact angle [26]. Similar to the theory of phoretic motion, within this approach the propulsion velocity is determined indirectly from the requirement that at the steady state the force exerted on the particle by the fluid vanishes. Based on the steady state concentration and velocity fields of the solvent, which were determined at the fixed temperature gradient for several values of the heat flux across the heated cap, the following was concluded: (i) if a single (PnP) droplet of preferred phase is formed at the heated cap, such that the cap is partially covered, the particle moves away from the cap due to body forces, which are localized at the droplet edges; (ii) if the temperature at the unheated part of the colloid surface increases above T_c and a droplet of opposite phase (water-rich) nucleates also there such that it covers uncapped surface partially, the particle moves towards the heated cap due to body force near the interface separating two droplets; (iii) if the demixed region completely encloses particle forming essentially a large symmetric droplet around it, the self-propulsion becomes negligible. We note that the wetting BCs employed in Refs. [10,24] do not account for critical adsorption, which is significant for temperatures close to the critical temperature. Thus, the existence of the adsorption layer at the unheated part of the Janus particle is completely neglected within this approach.

Here, we propose a description of the experimental system, which is based on the fluid particle dynamics method. Within this method, both the flow of the solvent and the motion of the particle are accounted for simultaneously such that the velocity of the particle can be computed directly. This provides a valuable complementary theoretical approach to the ones described above. The model takes care of the fact that the system is non-isothermal. The adsorption preferences of the two sides of the Janus particle are incorporated on a more microscopic level than in Refs. [10,24], i.e., by using effective surface interactions, which account for both wetting and critical adsorption. In order to shed light on contradictory experimental results concerning the direction of propulsion in relation to the adsorption preference of the two sides of the Janus colloid, we systematically study its various combinations as a function of temperature quench (heating power) and particle size. We consider both the critical and off-critical composition of a binary solvent. Our findings are compared with experimental observations and other theoretical results.

Simulation model

We consider a spherical Janus particle suspended in a binary liquid mixture. This liquid mixture has a lower critical point, above which it separates into two phases. A part of the particle surface is heated by an external source such as illumination by laser. As a results of local heating, a liquid mixture phase-separates locally near the surface of the particle[6,27,28].

We describe the particle by means of fluid particle dynamics method, which is a hybrid simulation treating with the lattice space and off-lattice space[29–35] We represent the particle with a smooth shape function as

$$\psi(\mathbf{r},\mathbf{x}) = \frac{1}{2}\left\{\tanh\left(\frac{R-|\mathbf{r}-\mathbf{x}|}{d}\right)+1\right\}. \quad (1)$$

Here $\mathbf{r}$ is the coordinate in the lattice space (the components of $\mathbf{r}$ are integers), and $\mathbf{x}$ is the position of the center of the particle in an off-lattice space (the components of $\mathbf{x}$ are floating point numbers). R is the radius of the particle and d represents the width of the smooth interface. In the limit of $d \to 0$, ψ is unity and zero in the interior and exterior of the particle, respectively. We also define the surface of the particle via the surface distribution as

$$\psi_{\rm sur} = d|\nabla\psi|. \quad (2)$$

The orientation of the Janus particle is given by $\mathbf{n}$ ($|\mathbf{n}|=1$).

In order to describe a binary mixture in an inhomogeneous temperature field T, we apply the dynamic van der Waals theory[25,36–40], to incompressible liquid mixtures of A- and B-components. We express the local concentration field of the A-component in the binary solvent as $\phi(\mathbf{r})$. The thermodynamic mixing energy $\mathscr{E}$ and entropy $\mathscr{S}$ in the system are written as

$$\mathscr{E}\{\phi,\mathbf{x},\mathbf{n}\} = \frac{1}{v_0^3}\int d\mathbf{r}e, \quad \mathscr{S}\{\phi,\mathbf{x}\} = \frac{1}{v_0^3}\int d\mathbf{r}s. \quad (3)$$

Here e and s are the energy and entropy per solvent molecule, and v_0 is a typical size of the solvent molecules. We assume that the local entropy has a form

$$s(\phi,\mathbf{x}) = k_{\rm B}(1-\psi)\left\{-\left(\frac{a}{2}\phi^2+\frac{b}{4}\phi^4\right)+\ln\left(\frac{\xi_0}{\lambda_T}\right)^3+1\right\}, \quad (4)$$

where a and b are positive constants. λ_T is the thermal de Broglie length, which is proportional to $T^{-1/2}$. The coefficient of $(1-\psi)$ is introduced since the entropy is defined only in the solvent. Domains of positive and negative ϕ represent the A-rich and B-rich phases, respectively. $\phi=0$ corresponds to the symmetric mixture, i.e., at the critical composition.

The local energy is given by

$$\begin{aligned} e(\phi,\mathbf{r},\mathbf{n}) &= (1-\psi)\left\{-\frac{\varepsilon}{2}\phi^2+\frac{K}{2}|\nabla\phi|^2+\frac{3}{2}k_{\rm B}T\right\} \\ &+ W(\mathbf{r}-\mathbf{x},\mathbf{n})\psi_{\rm sur}(\mathbf{r})\phi(\mathbf{r}) \\ &+ \frac{\chi_{\rm p}}{2}\{\phi(\mathbf{r})-\phi_{\rm p}\}^2\psi(\mathbf{r}) \end{aligned} \quad (5)$$

The first term in the right hand side of Eq. (5) represents the energy of the mixture and kinetic energy. K is the coefficient of the gradient term. ε represents the interaction energy. In our model, it is not a constant and can change with the temperature (see below). The second term represents the effective interaction of the binary solvent with the surface of a particle, which is defined by $\psi_{\rm sur}$ (Eq. (2)). W represents the adsorption preference (or wettability) of the particle surface. If $W<0$, the A-component with characterised by positive ϕ tends to wet the surface. To consider the heterogeneity of the surface, we set

$$W(\mathbf{r}-\mathbf{x},\mathbf{n}) = W_0 + W_1\mathbf{n}\cdot\frac{\mathbf{r}-\mathbf{x}}{|\mathbf{r}-\mathbf{x}|}, \quad (6)$$

where W_0 and W_1 are surface interaction constants (the material constants for the wetting). The third term of Eq. (5) is introduced to avoid the solvent invasion into the particle. $\chi_{\rm p}$ and $\phi_{\rm p}$ are its control positive parameters.

The time development of the local concentration field $\phi(\mathbf{r},t)$ obeys the following conservation equation,

$$\frac{\partial\phi}{\partial t} = -\nabla_i(\phi v_i) + \nabla_i\left\{D_0(1-\psi)\nabla_i\frac{\mu}{k_{\rm B}T}\right\} + \nabla_i\zeta_i, \quad (7)$$

where $\mathbf{v}$ is the fluid velocity field. D_0 is the diffusion constant in the bulk, and ζ is the thermal noise. Hereafter, the repeated indices are summed over. In the absence of thermal noise, the stationary state equation reduces to the Euler-Lagrange equation for the equilibrium mean-field order parameter profile.

μ is the local chemical potential, which is given by

$$\mu = -T\left(\frac{\delta\mathscr{S}}{\delta\phi}\right)_e, \quad (8)$$

where the functional derivative of the entropy functional is taken at fixed energy e (eqn. (5)). If there is no particle suspended in the binary mixture, μ is written as

$$\frac{\mu}{k_{\rm B}T} = -\tau\phi + b\phi^3 - \nabla\left(\frac{K}{k_{\rm B}T}\nabla\phi\right), \quad (9)$$

where $\tau = a - \varepsilon/k_{\rm B}T$ (see Appendix A).

The hydrodynamic equation for velocity $\mathbf{v}$ of the solvent is given by

$$\frac{\partial\rho v_i}{\partial t} = -\nabla_j(\rho v_i v_j) - \nabla_i p - \nabla_j\Pi_{ij} + \nabla_j\sigma_{ij} + F_i, \quad (10)$$

where ρ is the mass density, which is assumed to be constant. p is the pressure, which is determined to satisfy the incompressible condition $\nabla\cdot\mathbf{v}=0$. Π_{ij} is a reversible part of the stress tensor. Following the dynamic van der Waals theory, it is given by

$$\Pi_{ij} = \frac{K}{v_0^3}(\nabla_i\phi)(\nabla_j\phi). \quad (11)$$

σ_{ij} is the irreversible stress tensor, which is given by

$$\sigma_{ij} = \eta(\nabla_i v_j + \nabla_j v_i). \quad (12)$$

In this study, we assume that the viscosity depends on the particle

distribution via

$$\eta = \eta_s + (\eta_p - \eta_s)\psi, \tag{13}$$

where η_s and η_p are the solvent and particle viscosities. If $\eta_p \gg \eta_s$, the particle can be regarded as a solid particle.

F is the force field exerted on the fluid due to the particle. We assume

$$\mathbf{F}(\mathbf{r}) = \frac{\psi}{\Omega}\left(-\frac{\partial \mathscr{E}}{\partial \mathbf{x}}\right)_s + \frac{1}{2}\nabla \times \left\{\frac{\psi}{\Omega}\mathbf{n} \times \left(-\frac{\partial \mathscr{E}}{\partial \mathbf{n}}\right)_s\right\}, \tag{14}$$

where the partial derivatives of the energy are taken at fixed entropy s (eqn. (4)). In the above, we have used the fact that the energy $\mathscr{E} = \mathscr{F} + T\mathscr{S}$, where $\mathscr{F}$ is the free energy. Ω is the volume of the particle given by $\Omega = \int d\mathbf{r}\psi$. We note that Brownian motion is included in our approach. It arises because the order parameter (concentration of a binary solvent) is subjected to thermal noise and hence fluctuates. Hence, the total force exerted on the particle by fluid has a random component in it. The diffusive dynamics competes with the advection as given by Eq. (7).

The position and the orientation of the particle are transported by the flow according to

$$\frac{d}{dt}\mathbf{x} = \mathbf{V}, \tag{15}$$

$$\mathbf{V} = \frac{1}{\Omega}\int d\mathbf{r}\psi\mathbf{v}, \tag{16}$$

$$\frac{d}{dt}\mathbf{n} = \frac{1}{2\Omega}\int d\mathbf{r}\psi(\nabla \times \mathbf{v}). \tag{17}$$

The temperature field obeys the following equation

$$\frac{\partial T}{\partial t} = -\nabla_i(Tv_i) + \lambda\nabla^2 T - \alpha(T - T_\infty) + \frac{H(\mathbf{r})}{C_p}. \tag{18}$$

The first term of the right hand side of Eq. (18) is due to the convective flow. The second term is the thermal diffusion. Here, we assume all the materials have the same thermal diffusivity λ. $H(\mathbf{r})$ describes the local heat source and C_p is the specific heat. We assume that the particle surface is heated heterogeneously by external illumination. We set the heat source as

$$H(\mathbf{r}-\mathbf{x},\mathbf{n}) = H_0\psi_{sur}(\mathbf{r})\left\{1 + \mathbf{n}\cdot\frac{\mathbf{r}-\mathbf{x}}{|\mathbf{r}-\mathbf{x}|}\right\}, \tag{19}$$

where H_0 represents the heating power. The third term describes the dissipation to the bath, the temperature of which is T_∞. Without this term, the system is heated without bounds. $L = \sqrt{\lambda/\alpha}$ gives a characteristic length for decaying the temperature field to the bath. In experiments, L is considered to be comparable to the cell thickness.

Since in this study we consider near-critical solutions, we can safely assume that K/k_BT in Eq. (9) does not depend on T and set $K/k_BT = \nu_0^2$. We have checked that this approximation does not change our simulation results essentially. In order to be able to reproduce the equilibrium near-critical behavior of a binary solvent in the absence of a particle, we assume that τ in Eq.(9) depends linearly on T as $\tau = k_B(T - T_c)/(K/\nu_0^2)$, where T_c is the critical temperature of a binary solvent. We recall that in an isothermal solution, the bulk correlation length is given by $\xi \simeq \xi_0|\tau|^{-\nu}$ and the amplitude ξ_0 depends on coefficients in Eq. (9). Here we set $\xi_0 = \nu_0$, the molecular size appearing in Eq. (3). The coexistence curve in isothermal systems is given by $\tau_{cx} \simeq b\bar{\phi}^{1/\beta}$, so that the isothermal critical point is at $\bar{\phi} = 0$ and $\tau = 0$. $\bar{\phi}$ is the average concentration field ϕ. ν and β are standard critical exponents (both equal to 1/2 in mean field)[41]. If the temperature is uniform, the mixture with the lower critical point is phase-separated for $\tau \geq \tau_{cx}$, while it is mixed for $\tau < \tau_{cx}$.

We note that the interfacial tension is given by $\gamma \simeq \gamma_0|\tau|^{-\mu}$, where $\mu = \nu(d-1)$ (equal to 3/2 in mean field). We use the mean-field amplitude of the interfacial tension $\gamma_0 = 2^{3/2}k_BT/(\xi_0^2 b)$ in order to define a non-dimensional parameter $\Gamma = 3\gamma_0\xi_0/(2^{3/2}\eta_s D_0)$. This parameter gives the ratio of the third and fourth terms in Eq.(10), i.e., a typical amplitude of the hydrodynamic flow caused by the interface tension. The heat source parameter is also scaled as $h = k_B H_0 \xi_0^2/(\alpha C_p K)$. In the simulations, the lattice space is discretized with d, which is set to $d = \xi_0$ in this study. The time units is given by $t_0 = \xi_0^2/D_0$.

We use typical parameters as $v_0 = 2\,\mathrm{nm}$, $\eta_0 = 1\,\mathrm{mPa\cdot s}$, $D_0 \cong 1.1\times10^{-10}\,\mathrm{m^2/s}$, $\gamma_0 \cong 0.1\,\mathrm{mN/m}$, and $t_0 \cong 3.6\times10^{-8}\,\mathrm{s}$. We also set $\chi_p = 5$ in Eq. (5) and $b = 1$.

The particle motion and the concentration field are updated with a time increment $\Delta t = 0.005t_0$. Usually, the thermal diffusion constant λ is much larger than the diffusion constant for the concentration field D_0. Thus, it is difficult to simulate the concentration and temperature fields with the same time increment. We iterate the thermal diffusion equation by 100 steps without updating the concentration and flow fields. Its time increment is set to $\Delta t = 0.005d^2/\lambda$. The diffusion constant ratio in our system correspond to $D_0/\lambda = 10^{-2}$. Although this ratio is still lager than that in actual mixtures, we confirmed that the temperature field reaches almost the steady state in each time step for the concentration field. The decaying length of the temperature field is set to $L = 10d$. The hydrodynamic flow (Eq. (10)) is solved by means of Makers and Cell method with the staggered lattice. In Eq. (7), the Gaussian random noises of $\sqrt{\langle|\zeta|^2\rangle} = 0.2\xi_0/t_0$ are imposed in each lattice.

We employ five kinds of Janus particles with different wetting parameters in Eq. (6). They are summarized in table 1. Two types of them are uniform. A NN (neutral head-neutral tail)-particle of $W_0 = W_1 = 0$ has no preference for one component of a binary solvent over the other (neutral in wetting), while a WW (wetting head-wetting tail)-particle of $W_0 = -2$ and $W_1 = 0$ prefers the A-components. The other three have heterogeneous wettabilities. The head side of a WN (wetting head-neutral tail)-particle of $W_0 = -1$ and $W_1 = -1$ prefers the A-component, while its tail side is neutral. On the other hand, the head side of a NW (neutral head-wetting tail)-particle of $W_0 = -1$ and $W_1 = 1$ is neutral, and its tail prefers the A-component. The last particle (WW′) of $W_0 = 0$ and $W_1 = -2$ prefers the A-component on its head, while it prefers the B-component on its tail.

We employ a three-dimensional square cell of $(128d)^3$ with periodic boundary conditions and the particle radius is set to $R = 8d$

type	W_0	W_1	head preference	tail preference
NN	0	0	neutral	neutral
WW	-2	0	A-component	A-component
WN	-1	-1	A-component	neutral
NW	-1	1	neutral	A-component
WW′	0	-2	A-component	B-component

Table 1 The wetting properties of five types of simulated Janus particles.

if we do not mention them explicitly.

Results

Temperature field

We place a WW-particle of $R = 8d$ in a symmetric mixture of $\bar{\phi} = 0$. The particle head is oriented towards $\mathbf{n} = (0,0,1)$. The background temperature is set to $\tau_\infty = -1$, so that a binary solvent with a lower critical point is in a one-phase mixed state when $h = 0$.

At $t = 0$, we turn on illumination of the system by imposing $h > 0$. After a sufficiently long heating, the system reaches a steady state, in which the particle moves along $\mathbf{n}$ with a constant velocity. Figure 1(a) shows a snapshot of the steady state temperature field under $h = 30$ at $t = 500t_0$. The three dimensional simulation result is sliced in the xz-plane passing through the particle center. In Fig. 1(a), the WW-particle propels upward towards its heated part. In Fig. 1(b), we also plot the profiles of the temperature field for several h along the straight line parallel to $\mathbf{n}$ through the particle center. $z/R = 1$ and $z/R = -1$ correspond to the head and tail surfaces, respectively. Since the head side of the particle surface is heated more strongly than the tail side, the temperature field has a peak at $z/R = 1$ and decays to the background of $\tau_\infty = -1$. In the inset of Fig. 1(b), we plot the peak height as function of h. It is shown that the peak height increases almost linearly with the heating power h. As shown in the inset, the peak temperature exceeds the critical temperature $\tau_{\rm cx}(\bar{\phi} = 0) = 0$ when $h > h_{\rm T} (\cong 16.3)$. We note that the temperature field is almost independent of the wettabilities, and on $\bar{\phi}$.

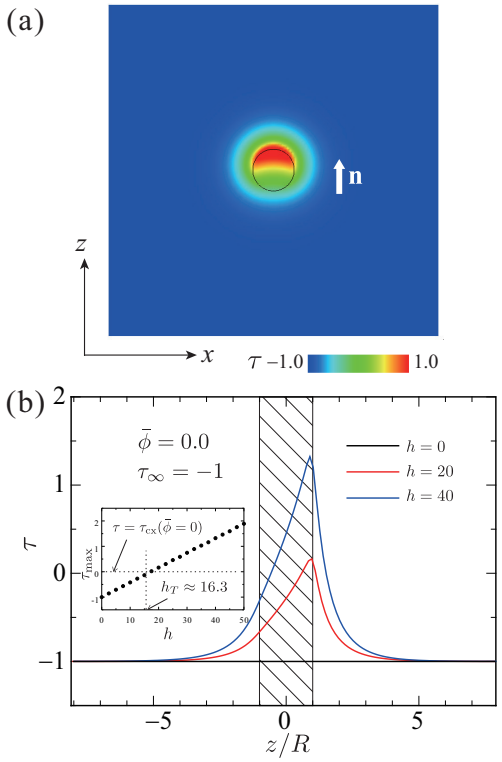

Fig. 1 (a) A snapshot of the temperature field around a WW-Janus particle. The background temperature is $\tau_\infty = -1$ and the heating power is $h = 40$. The average concentration is $\bar{\phi} = 0.0$. The black circle represents the particle, which is oriented upward, i.e., the heated particle head is oriented towards $\mathbf{n} = (0,0,1)$. (b) The profiles of the temperature field in the case of $\tau_\infty = -1$. The heating power varies. The hatched region indicates the particle inside. In the inset, the peak height of the temperature profile $\tau_{\rm max}$ is plotted versus h.

WW-particle in symmetric mixtures

Figure 2(a) and (b) show typical snapshots of the concentration field at $t = 500t_0$ around the WW-particle in the symmetric mixture under $h = 0$ and $h = 40$, respectively.

We recall that the equilibrium adsorption profiles at the spherical particle suspended in the supercritical mixed phase of a binary solvent, were studied theoretically in Refs.[42–45]. Close to the critical point of demixing, due to the phenomenon of critical adsorption these profiles become universal and for $R > \xi$ decay algebraically with the distance from the surface r up to $r \lesssim \xi$. In comparison with the critical adsorption profile at the planar wall, this algebraic decay is faster, i.e., with the exponent $2\beta/\nu$ as compared to β/ν for a planar wall. For larger r the decay becomes exponential $\sim \exp(-r/\xi)$. In our simulations, the order parameter is conserved and the system is finite, therefore, we cannot expect full agreement with theoretical predictions (the latter concern infinite system and, hence, a non-conserved order

parameter). However, the decay of the equilibrium ($h = 0$) order parameter profiles obtained from our simulations is to a good approximation exponential. Notice that for the background temperature $\tau_\infty = -1$, the bulk correlation length $\xi = \xi_0 \ll R$. Hence, the range of algebraic decay cannot be observed at this temperature.

In Fig. 2(c), we show the profiles of the concentration field along the straight line parallel to **n** through the particle center.

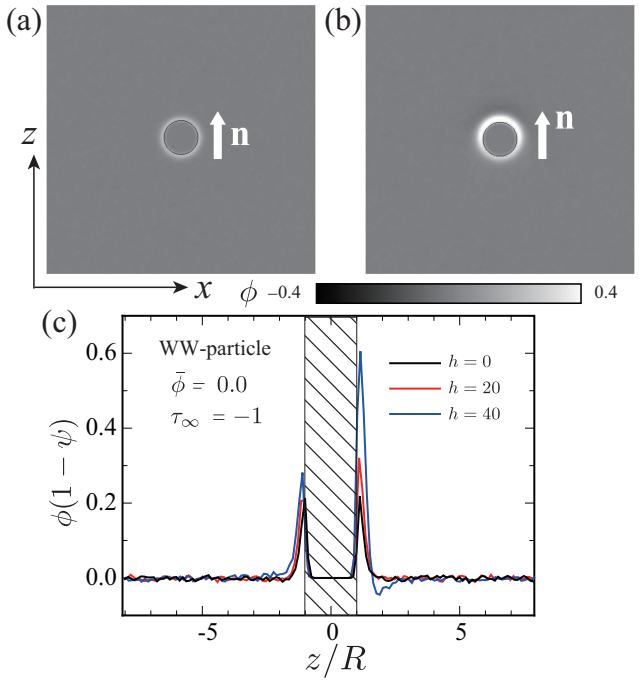

Fig. 2 (a) and (b) Typical snapshots of the concentration field ϕ around a WW-particle in the critical mixture of $\bar{\phi} = 0$ and $\tau_\infty = -1$. The heating power is $h = 0$ in (a) and $h = 40$ in (b). (c) The profiles of the concentration field around the WW-particle in the critical mixture. The hatched region marks the interior of the particle. The heating power varies.

In order to better assess the dependence of the concentration field on the heating power, in Fig. 3(a) we plot the quantities that measure the degree of the concentration variation. They are calculated as

$$\delta\phi_{\rm f}^2 = \int_{(\mathbf{r}-\mathbf{x})\cdot\mathbf{n}>0} d\mathbf{r}\{\phi(\mathbf{r}) - \bar{\phi}\}^2 \frac{\{(\mathbf{r}-\mathbf{x})\cdot\mathbf{n}\}^2}{|\mathbf{r}-\mathbf{x}|^2}, \tag{20}$$

$$\delta\phi_{\rm r}^2 = \int_{(\mathbf{r}-\mathbf{x})\cdot\mathbf{n}<0} d\mathbf{r}\{\phi(\mathbf{r}) - \bar{\phi}\}^2 \frac{\{(\mathbf{r}-\mathbf{x})\cdot\mathbf{n}\}^2}{|\mathbf{r}-\mathbf{x}|^2}. \tag{21}$$

Here, the degree of the concentration variations is defined separately for the front and rear sides of the particle ($\delta\phi_{\rm f}^2$ and $\delta\phi_{\rm r}^2$), respectively.

Because of the homogenous surface interaction, an adsorption layer rich in the A-component is formed uniformly at the particle surface for $h = 0$, as shown in Figs. 2(a) and (c). Under illumination the concentration field becomes more heterogeneous at the surfaces - see Figs. 2(b), 2(c) and 3(a). Furthermore, upon increasing the heating power the concentration field in the front region develops more quickly than that in the rear region. This is because the susceptibility of the binary solvent to the wetting interaction is enhanced around the head where the temperature is increased. When τ exceeds the critical temperature $\tau_{\rm cx}$ largely, the solvent is phase-separated locally around the particle. We discuss these behaviors below again.

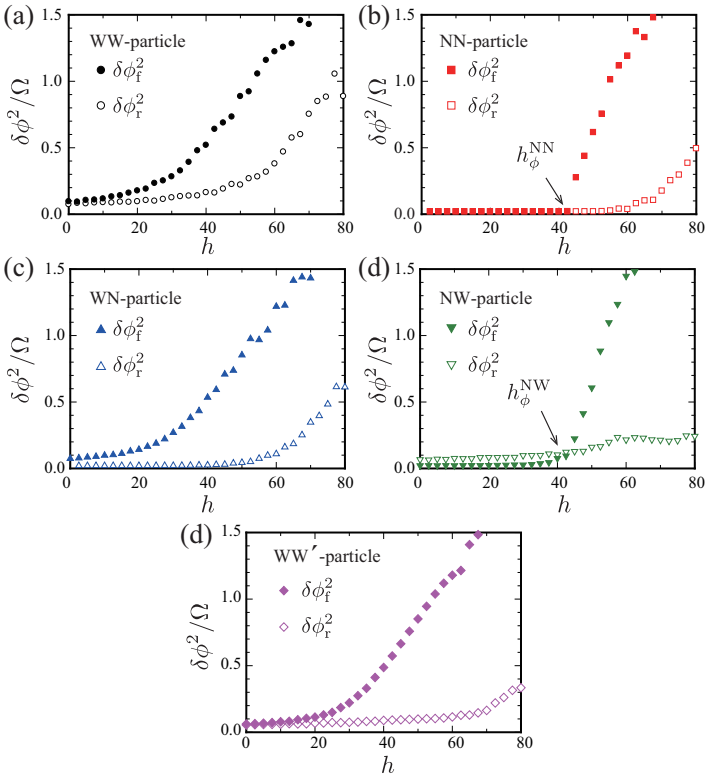

Fig. 3 Plots of the degree of the concentration inhomogeneities with respect to the heating power. They are calculated separately for the front and rear regions of the (a) WW-, (b) NN-, (c) WN-, (d) NW- and (e) WW′-particles.

In Fig. 4(a), we show the flow field at $t = 500t_0$. It corresponds to Figs. 1(a) and 2(a), and indicates that the particle moves towards its head. In Fig. 4(b), we plot the temporal change in the total force. The total force is calculated from the acceleration of the particle as $F_{\rm tot} = M|d\mathbf{V}/dt|$, where $M(= 4\pi a^3\rho/3)$ is the particle mass. It is scaled by the propelling force $F_{\rm pro}$ at $t = 500t_0$. The propelling force $F_{\rm pro}$ is determined in another simulation with the same parameters. We fix the particle at the initial position with a spring potential, $K(\mathbf{x}-\mathbf{x}_0)^2/2$, where $K = 10k_{\rm B}T/d^2$ and $\mathbf{x}_0 = \mathbf{x}(t=0)$[30]. Under illumination, the spring get stretched by the propelling force. Where the particle motion is stopped, the propelling force is balanced by the spring force, so that its strength is given by $F_{\rm pro} = |K(\mathbf{x}-\mathbf{x}_0)|$. In the absence of the spring potential, after illumination is switched on the total force $F_{\rm tot}$ initially increases with time. This increase is connected with the process of formation of the adsorption layer. After some time, the total force reaches a maximum and then decays to zero. The total force contains the propelling force and the viscous resistance force. In the earlier stage, the speed of the particle is low so that

the resistance force is weak and the propelling force is dominant. In the late stage, on the other hand, the total force goes to zero, which indicates the propelling force is balanced by the viscous force. Fig. 4(b) ensures the flow pattern in Fig. 4(a) is at the steady state.

In Figs 4(c) and (d), we plot the velocity profiles along the lines passing through the particle center parallel to the x- and z-directions, respectively. The hatched regions indicate the particle and the broken lines indicate the particle velocity. These figures demonstrate that although the flow inside the particle is not homogeneous due to our numerical scheme, the flow field almost satisfies the non-slip boundary conditions at the particle surface. In other words, discontinuous jumps or steep changes of the flow field typical for thermo- or diffusio-phoresis are not observed. The flow is induced mainly by the mechanical stress due to the concentration variation. In Fig. 4(e), the stress field due to the concentration variation Π_{ij} is depicted by line segments. The length and the orientation of these line segments indicate the eigenvalues of Π_{ij} and the corresponding eigenvectors. It is instructive to relate the spatial distribution of this stress field to the concentration profile shown in Fig. 2(c). The concentration profile in the front region of the particle does not look like a wetting film profile, which typically is constant up to some distance ℓ from the surface (defining wetting film thickness) followed by a rapid decay to the bulk value. Rather, the concentration decays from its maximum value close to the surface in a gradual way over a distance $z \approx R$ so that no sharp liquid-liquid interface is observed. Accordingly, the stress field Π_{ij} is not localized near the outer edge of the adsorption layer. We can see that in the whole front region of the particle the line segments (along which a contraction force works) are relative long, i.e., the stress Π_{ij} is larger there. The orientation of these line segments is tangential to the interfacial region, which is broad. Due to the temperature gradient, both the length of line segments and their orientation vary along the surface of a particle. This variation gives rise to hydrodynamic flow in a way similar to the Marangoni effect, e.g., such as the thermo-capillary effect in liquid droplets[46].

As is shown in Fig. 4(a), the induced flow pushes the particle toward its head side. Although we impose random fluctuation in Eq. (7), it is not too strong so that the particle shows a straight motion. Figure 5(a) plots the particle velocities in the steady state as a function of the heating power for two values of the ambient temperature $\tau_\infty = -1$ and 0. The particle velocity is calculated from Eq. (16) as $V_\parallel = \mathbf{V} \cdot \mathbf{n}$. The positive value of the velocity means the motion of the particle toward its head. For the WW-particle, the particle velocity increases monotonically upon the increase of the heating power. Also, the motion in the solvent with $\tau_\infty = 0$ (at its critical temperature) is faster than that with $\tau_\infty = -1$. This is because for $\tau_\infty = 0$ the temperature around the whole colloid is larger than T_c and hence the system is much more susceptible to the perturbation by the surface interaction. Due to resultant large concentration variation, the particle can propel faster.

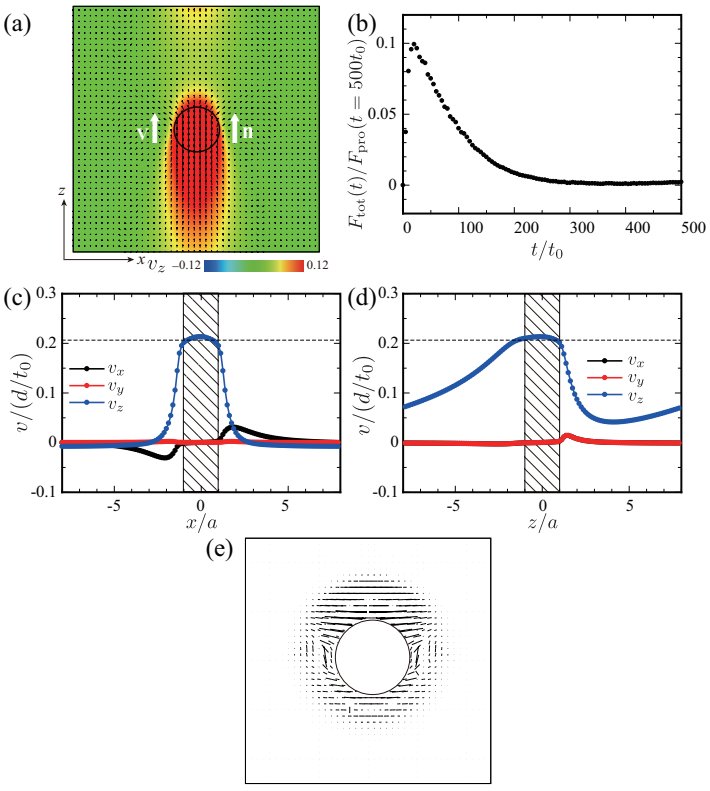

Fig. 4 (a) A snapshot of the flow field around a WW-particle at the steady state ($t = 500t_0$). The arrows represent the local velocity field and the background color shows the z-component of the flow field. The heating power is $h = 40$. (b) The temporal change in the total force acting on the WW-particle. In the late stage, it goes to zero, which indicates that the propelling force is balanced to the viscous force. (c) and (d) The flow profiles along the lines through the particle center parallel to the (c) x- and (d) z-directions. (e) The corresponding stress field stemming from the concentration variation. The length and the orientation of the segment represents the eigenvalue and eigenvector of the stress field tensor Π_{ij}. A contraction force works locally along the segment orientation.

NN-particle in symmetric mixture

Figure 5(b) shows the particle velocities of the NN-particle. The other parameters are the same as those in Fig. 5(a). In contrast to the motion of the WW-particle, the NN-particle does not show any motion below the threshold $h_V^{NN}(\cong 42.5)$ for $\tau_\infty = -1$. Above h_V^{NN}, the particle velocity increases with h. For $\tau_\infty = 0$, the particle speed is larger than that for $\tau_\infty = -1$, as in the case of the WW-particle.

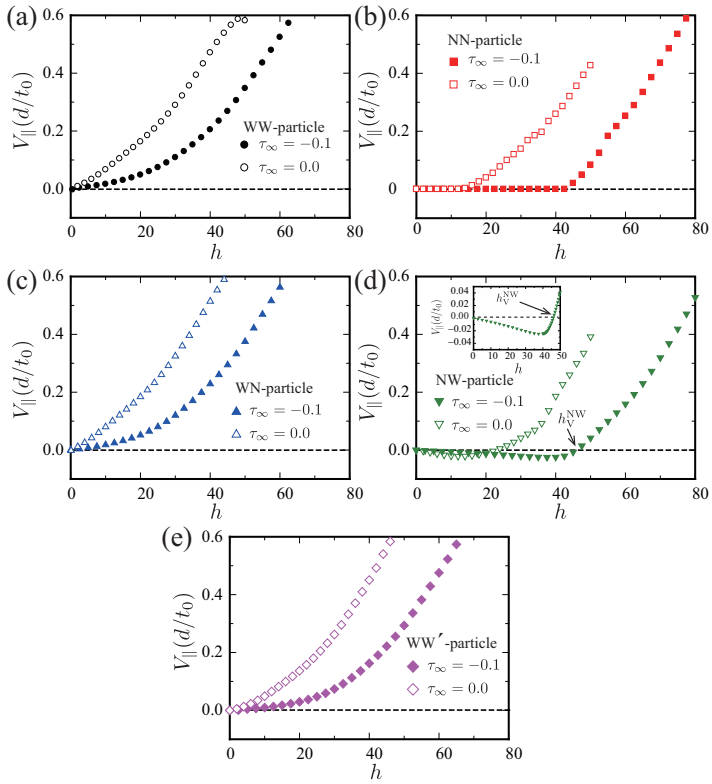

Fig. 5 Plots of the particle velocity with respect to the heating power h for (a) WW-, (b) NN-, (c) WN-, (d) NW- and (e) WW′- particle. The average concentration is $\bar{\phi} = 0.0$ and the background temperature is $\tau_\infty = -1$ (filled symbols) and $\tau_\infty = 0$ (open symbols). In (d), the detailed behavior of the motion inversion for the NW-particle is shown in the inset.

For a NN-particle in a symmetric mixture, none of the A- and B- components is preferred. Thus, the domains of positive and negative ϕ are formed with the same probability, so that the concentration profiles themselves are not so useful to see the concentration variation. Instead of the concentration profiles, we show the degrees of the concentration variations $\delta\phi_f^2$ and $\delta\phi_r^2$ for the NN-particle as functions of h in Fig. 3(b). The background temperature is $\tau_\infty = -1$. As indicated by the arrow, the degree of the concentration variation in the front region $\delta\phi_f^2$ also has a threshold h_ϕ^{NN}, below which it is small and comparable to that due to the thermal noise. Above h_ϕ^{NN}, $\delta\phi_f^2$ is increased as the heating power is increased. This threshold power is consistent with the above threshold power for the particle motion, *i.e.*, $h_V^{NN} \cong h_\phi^{NN}$. It is reasonable since the hydrodynamic flow and the resultant particle motion are caused by inhomogeneities in the concentration field. Also, the concentration variation around the head is larger than that around the tail, $\delta\phi_f^2 > \delta\phi_r^2$. Thus we conclude that the concentration variation in the front region of the particle plays a dominant role in inducing the hydrodynamic flow.

It is expected that the phase separation occurs immediately when the local temperature exceeds the phase separation temperature τ_{cx}. However, our simulations indicate that upon increasing h, a formation of A- or equivalently B-rich region around the colloid occurs if the temperature near the head is considerably higher than τ_{cx}. In the case of $\tau_\infty = -1$, the temperature at the head surface exceeds τ_{cx} when the illumination of $h = h_T(\cong 16.3)$ is applied (see the inset of Fig. 1(b)). However, the fluctuations of the concentration are of the order of the noise (therefore not distinguishable from zero in Fig. 3(b)) and the NN-particle does not move (see Fig. 5(b)). The domains rich in A or B components are formed only when the local temperature becomes sufficiently higher than the phase transition temperature so that the fluctuations are larger than the noise and can grow.

As shown in Fig. 3(a), the degrees of the concentration variation for the WW-particle do not have thresholds, in contrast to those for the NN-particle. This is due to the surface interaction, which enhances formation of preferred phase near the surface in a way similar to surface-directed spinodal decomposition[47,48].

Particles with heterogeneous wettabilities

Next we consider particles with heterogeneous wettabilities such as WN-, NW- and WW′-particles defined in Table 1. We have found that they also self-propel along **n** under the illumination, and that the details of the motion depend on the surface interactions. The steady state velocities of WN-, NW- and WW′ particles as function of the heating power are shown in Fig. 5(c), (d) and (e), respectively. The average concentration is $\bar{\phi} = 0$ and the background temperature is $\tau_\infty = -1$ and 0.*

As can be seen in Figs. 5(c) and (e), the WN- and WW′-particles self-propel even for small values of h and their velocities are close to that of the WW-particle. On the other hand, the velocity of the NW-particle is similar to that of the NN-particle. Interestingly, out of 5 types of Janus particles considered here, only the NW-particle exhibits change in the direction of self-propulsion, as shown in Fig. 5(d). For a small heating power, the particle moves toward the tail, i.e., in the opposite direction than other types of Janus particles. In the case of $\tau_\infty = -1$, for the heating power larger than the threshold value $h_V^{NW}(\cong 46)$, the direction of motion is switched and the particle moves toward the head. This crossover power h_V^{NW} is roughly close to the threshold for the NN-particle motion in Fig. 5(b), $h_V^{NN} \approx h_V^{NW}$. We note that similar inversions of the direction of motion has been also observed in the experiment[10] and theory[10,23,24]. We discuss this issue in more detail in Sec. 4.

In Figs. 3(c), (d) and (e) we show the degrees of the concen-

* In our simulations, particles with the heterogeneous wettabilities show directed motion with a small velocity even in the absence of illumination. This is an artifact of the numerical scheme In the following we subtract this velocity from the steady state velocity determined for $h > 0$.

tration variations for the WN-, NW- and WW′-particles, respectively. For the WN-particle, the concentration variation $\delta\phi_{\rm f}^2$ at the front of the particle agrees with that for the WW-particle. On the other hand, the concentration variation $\delta\phi_{\rm r}^2$ at the rear of the WN-particle is similar to that for the NN-particle. As noted above, the temperature field is almost independent of the surface properties. Thus, the differences between $\delta\phi_{\rm f}^2$ and $\delta\phi_{\rm r}^2$ are entirely due to distinct adsorption preference of the surface. We note that the concentration variation around the head side is always larger than that around the tail side, $\delta\phi_{\rm f}^2 > \delta\phi_{\rm r}^2$, for the WN-particle.

This is different for the NW-particle, if the heating power is small. In such a case, $\delta\phi_{\rm r}^2$ is larger than $\delta\phi_{\rm f}^2$. This is because the tail side has a preference for the A-component, whereas the head side is neutral. However, when h is increased above $h_\phi^{\rm NW}(\cong 44)$, the temperature near the head becomes high enough to induce the local phase separation. This results in a steep growth of $\delta\phi_{\rm f}^2$ - as in the case of the NN-particle. Finally, for $h > h_\phi^{\rm WN}$ $\delta\phi_{\rm f}^2$ becomes larger than $\delta\phi_{\rm r}^2$. In Fig. 6, we show the snapshots of the sliced concentration fields ((a) and (b)), the tensorial field ((c) and (d)), and the flow field ((e) and (f)), below and above the crossover $h_\phi^{\rm NW}$. Below the crossover, a thin adsorption layer rich in A-component is formed on the rear surface, while variation in concentration around the head is hardly visible. As the heating power is increased, a rather thick B-component rich layer is created on the front surface. Comparing Fig. 6(c) and (d) we can see that the dominant stress shifts from the rear (Fig. 6(c)) to the front (Fig. 6(c)) of the particle, reflecting the change in the concentration field. In Figs. 6(e) and (f) it is demonstrated that the resultant hydrodynamic flow changes its direction. For the particles other than the NW-particle, we have not observed such a crossover of the concentration variation, and the motion inversion.

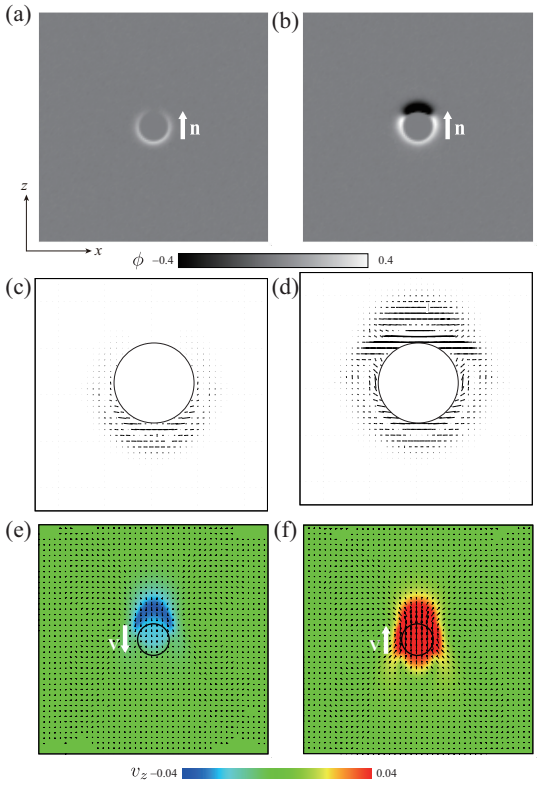

Fig. 6 (a) and (b) Snapshots of the concentration field around the NW-particle. The heating power is $h = 30(< h_\phi^{\rm NW})$ in (a) and $h = 50(> h_\phi^{\rm NW})$ in (b). The average concentration is $\bar{\phi} = 0.0$ and the background temperature is $\tau_\infty = -1$. (c) and (d) show the corresponding stress fields Π_{ij} due to the concentration variation. The heating power is $h = 30$ in (c) and $h = 50$ in (d). A contraction force is exerted along the line segment and its strength is proportional to the line segment length. (e) and (f) show the corresponding flow field around the NW-particle. The arrows represent the local velocity field and the background color shows the z-component of the flow field. The heating power is $h = 30$ in (e) and $h = 50$ in (f).

Off-critical average concentrations

Next we study self-propulsion of the WW-particle suspended in the asymmetric binary mixture, i.e., at off-critical $\bar{\phi} \neq 0$ average concentrations. In Fig. 7 we plot the average particle velocities as function of $\bar{\phi}$ for $h \geq 10$ and $\tau_\infty = -1$. One might expect that the particle motion is the fastest at $\bar{\phi} = 0$. This is because at the critical concentration the phase separation temperature $\tau_{\rm cx}$ is the lowest so that the temperature quench is the deepest. Accordingly, the concentration gradients and hence the hydrodynamic flow should be the largest. Surprisingly, our simulations show that the self-propulsion velocity is notably larger in the highly asymmetric mixtures. This observation indicates that concentration gradients develop more strongly for off-critical concentrations than for the near-critical ones.

We note that for surfaces that are adsorptionwise neutral, one can expect differences in the onset of self-propulsion for off-critical concentrations as compared to the critical concentration. This is because dynamics of phase separation is distinct in these two cases, i.e., it is associated with nucleation for off-critical concentration and with spinodal decomposition for the critical concentration. For surfaces with preferential adsorption, like WW-particle, for both off-critical and critical concentration one ob-

serves the so called surface-directed phase separation characterized by formation of homogeneous surface layers that propagate into the bulk[27,28]. Therefore, the results shown in Fig. 7 cannot be explained by differences in the dynamics of phase separation.

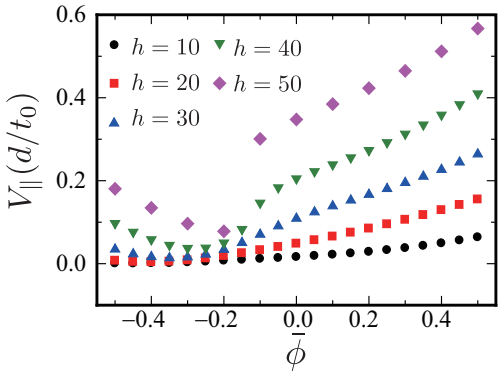

Fig. 7 Self-propulsion velocity of a WW-particle as function of the average concentration $\bar{\phi}$ for four values of the heating power h.

In Figs. 8(a) and (b) we plot the concentration profiles for $\bar{\phi} = 0.4$ and -0.4. The snapshots corresponding to these profiles are presented in (c) and (d). By comparing Figs. 2(c),(a) with Figs. 8(a),(c) and Figs. 8(b),(d), one can see that concentration fields are indeed more inhomogeneous in the asymmetric mixtures than in the symmetric mixture. Because the particle surface prefers the A-component of the binary solvent, both in the symmetric ($\bar{\phi} = 0.0$) and in the A-rich mixture ($\bar{\phi} = 0.4$), the A-rich domain forms also near the (colder) tail surface. However, the thickness of the adsorption layer is considerable larger for $\bar{\phi} = 0.4$ than that for $\bar{\phi} = 0$ (see Fig. 2(b)).

In the B-rich mixture (see Figs. 8(b),(d)), a domain rich in B-component is formed near the surface. This is rather surprising, because the surface prefers the A-component of a mixture. We note that the spatial extent of the concentration variation in the B-rich mixture is roughly the same as that in the A-rich mixture, i.e., the concentration profile for the B-rich mixture reflected with respect to the vertical axis almost overlap with that for the A-rich mixture (not shown here).

When the concentration inhomogeneity $\delta\phi = \phi - \bar{\phi}$ is small in the early stage of the phase separation, the concentration diffusion flux $\mathbf{J}_\phi$ outside the particle can be approximated using Eq. (9) as

$$\mathbf{J}_\phi \approx -D_0 \left\{ \left(-\tau + 3b\bar{\phi}^2 - \xi_0^2 \nabla^2 \right) \nabla\delta\phi - \bar{\phi}\nabla\tau \right\}. \qquad (22)$$

In isothermal systems, the second term in the right hand side of Eq. (22) is absent and the first term induces the phase separation. The second term describes the flux of the concentration field due to the temperature gradient, i.e., the Soret effect. In our model, the direction of the flux due to the Soret effect depends on the average concentration $\bar{\phi}$. Therefore, although the surface interactions with $W < 0$ prefer A-component of a mixture, in the B-rich mixture the Soret effect can be more important and the domain of the B-component can be formed near the surface of the particle. In the symmetric mixture ($\bar{\phi} = 0$), this effect is not relevant in the early stage, since $-\bar{\phi}\nabla\tau = 0$.

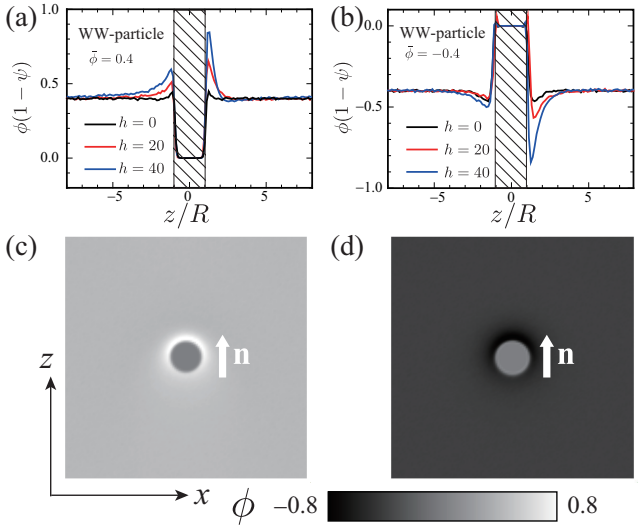

Fig. 8 (a) and (b) The profiles of the concentration field around the WW-particle along the particle orientation in asymmetric mixtures. The average concentration is $\bar{\phi} = 0.4$ in (a) and $\bar{\phi} = -0.4$ in (b). The heating power is varied. (c) and (d) Corresponding snapshots of the concentration field around the WW-particle in asymmetric mixtures. ((c) $\bar{\phi} = 0.4$ and (d) $\bar{\phi} = -0.4$.) the heating power is $h = 40$.

As one can see in Fig. 7, the self-propulsion velocity has a minimum at $\bar{\phi} = -0.2$, not at $\bar{\phi} = 0.0$. This shift is due to the surface interaction of the WW-particle. At $\bar{\phi} = -0.2$, the surface interactions, which prefers the A-rich component, are almost balanced by the Soret diffusion, in which the B-component is attracted to the surface .

Particle size dependence

Finally, we examine the particle size dependence of the self-propulsion velocity in our model. In Fig. 9 we plot the self-propulsion velocity for the WW-particle at the average concentration $\bar{\phi} = 0.0$ and the background temperature $\tau_\infty = -1$. The heating power is $h = 40$. We find that small particles, with a radius below $R = 4d$, does not move. Larger particles self-propel with velocity, which increases with the particle radius in a nonlinear way. Such behavior is consistent with the mechanism of self-propulsion due to the Marangoni-like effect, which is proportional to the surface area heated by illumination. Because the total heating power is expected to be proportional to R^2, if the particle is small, the temperature increase is not sufficiently large to induce phase separation of the binary solvent around the particle. Hence, the small particle does not propel under this heating power. Larger particles show self-propulsion. Because the friction force against the particle motion growths linearly with R, i.e., slower than the Marangoni-like effect, the particle motion becomes faster for a large particle. This result is consistent with the experimental observations (Fig. 4 in Ref.[6] and Fig. 1(f) in Ref.[10]). Note the difference with the catalytic self-propellers, for which the velocity is inversely proportional to the radius at given fuel concentration and the thickness of the catalytic cap[49].

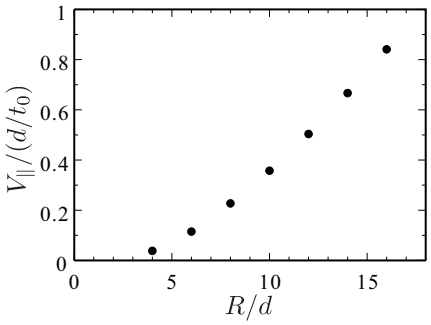

Fig. 9 The dependence of the steady state velocity of the WW-particle on the particle radius. The average concentration is $\bar{\phi} = 0$ and the heating power is $h = 40$.

Conclusions

We conclude that the mechanism leading to a directed motion of a Janus particle with heated hemisphere in the near-critical binary solvent, bears some similarity to the Marangoni effect. The point of similarity is that the flow (which pushes the particle) is induced by a gradient of the stress tensor along the particle surface. This mechanical stress results from the concentration variations within the adsorption domain (droplet) formed at the surface of a particle. Due to the inhomogeneous temperature field, the concentration variations are asymmetric around the particle. These findings are consistent with the results of Samin *et al.* reported in Ref.[10,24], although the hydrodynamic equation studied by these authors differs from Eq. (10). However, there is an important difference concerning particles with adsorbing surfaces (nonzero wetting parameters in Eq. (6)). Our model predicts correctly formation of critical adsorption layers at the unheated hemisphere, even if the temperature at this hemisphere is lower than T_c (see Fig, 2(b)); this is consistent with observations made within purely diffusive dynamics[27,28]. Critical adsorption phenomenon is not accounted for in the approaches of Samin *et al.*[10,24] and of Würger[23]. We have found that concentration gradients are considerably larger at the heated hemispheres (see Fig. 3). This holds also for the adsorptionwise neutral hemispheres - if the heating power h is sufficiently big. The Janus particle moves towards this hemisphere around which the concentration variations are larger. For all studied types of a Janus particle, except of the NW-particle at low heating powers, this is always towards the heated hemisphere. The NW-particle at low heating powers moves in the opposite direction, because for small h the concentration variations at the strongly adsorbing unheated hemisphere are larger than at the neutral heated side.

We would like to emphasize that in our model, contrary to results reported in Refs.[10,24], the stress due to the concentration gradients is not localized at the edge of a droplet or at the liquid-liquid interface between two droplets. Rather, due to a gradual decrease of the concentration profile from the surface of a particle, the mechanical stress occurs in the whole droplet. We have checked that the total force exerted by the fluid on the WW-particle vanishes at the steady state. This is consistent with the requirement of force free motion of the colloid, which was used in Refs.[10,24] to determine the particle velocity. Within our approach, the solid particle is approximated by a viscous particle with a shape that smoothly decays to zero on the length scale given by d. Accordingly, the velocity is not constant inside the particle but has a profile. Therefore non-slip boundary conditions are achieved only approximately, but deviations are very small ($\simeq$3% for the WW-particle at $h = 40$).

Concerning direction of the particle motion, our results agree with experimental observations for a silica particle with hydrophobic-functionalized cap in a water-2,6 lutidine mixture[5,6], and for a silica particle with a a hydrophobic carbon cap in a PNP mixture[10] at larger illumination intensities, where the shape of the adsorbed droplet (Fig. 3(d) in Ref.[10]) is similar to the one for the WN-particle (not shown here). The case of a silica particle capped with the hydrophilic-functionalized gold, which move away from the cap in the water-2,6 lutidine mixture[5,6] is not consistent with the findings of the present paper. However, we have not explored the full range of wetting parameters and of the decay length of the temperature field, which might influence the results. Note also that due to computational costs, we have studied rather small particles - in the adapted units they are of the size of nanoparticles and their speed is much larger than that observed for micro-sized particles.

An important result of our study is that the speed of self-propulsion can be significantly increased by using a binary solvent with off-critical compositions. Interestingly, the direction of motion depends on the spatial dimension of a system - in two dimensions it is exactly opposite to the one in three dimensions. Finally, we note that our results may also be useful for prediction of the behavior of Janus particles when the mixture undergoes bulk phase separation. Normal colloids partition into the preferred phase while Janus particles tend to behave like surfactants[50].

Conflicts of interest

There are no conflicts to declare.

Acknowledgements

The work by AM has been supported by the Polish National Science Center (Harmonia Grant No.2015/18/M/ST3/00403). T.A. acknowledges the support from JSPS KAKENHI Grants Numbers JP25000002 and JP17K05612, and JST CREST Grant No. JPMJCR1424, Japan.

References

1 H.-R. Jiang, N. Yoshinaga and M. Sano, *Phys. Rev. Lett.*, 2010, **105**, 268302.
2 R. Golestanian, *Phys. Rev. Lett.*, 2012, **108**, 038303.
3 K. Kroy, D. Chakraborty and F. Cichos, *The European Physical Journal Special Topics*, 2016, **225**, 2207–2225.
4 C. Bechinger, R. Di Leonardo, H. Löwen, C. Reichhardt, G. Volpe and G. Volpe, *Rev. Mod. Phys.*, 2016, **88**, 045006.
5 G. Volpe, I. Buttinoni, D. Vogt, H.-J. KÃijmmerer and C. Bechinger, *Soft Matter*, 2011, **7**, 8810–8815.
6 I. Buttinoni, G. Volpe, F. KÃijmmel, G. Volpe and C. Bechinger, *Journal of Physics: Condensed Matter*, 2012, **24**, 284129.

7 J. R. Howse, R. A. L. Jones, A. J. Ryan, T. Gough, R. Vafabakhsh and R. Golestanian, *Phys. Rev. Lett.*, 2007, **99**, 048102.
8 D. F. B. Haeufle, T. Bäuerle, J. Steiner, L. Bremicker, S. Schmitt and C. Bechinger, *Phys. Rev. E*, 2016, **94**, 012617.
9 C. Lozano, B. ten Hagen, H. LÃűwen and C. Bechinger, *Nature Communications*, 2016, **7**, 12828.
10 J. R. Gomez-Solano, S. Samin, C. Lozano, P. Ruedas-Batuecas, R. Roij and C. Bechinger, *Scientific Reports*, 2017, **7**, 14891.
11 J. R. Gomez-Solano, A. Blokhuis and C. Bechinger, *Phys. Rev. Lett.*, 2016, **116**, 138301.
12 N. Narinder, C. Bechinger and J. R. Gomez-Solano, *Phys. Rev. Lett.*, 2018, **121**, 078003.
13 F. Kümmel, B. ten Hagen, R. Wittkowski, I. Buttinoni, R. Eichhorn, G. Volpe, H. Löwen and C. Bechinger, *Physical review letters*, 2013, **110**, 198302.
14 B. Ten Hagen, F. Kümmel, R. Wittkowski, D. Takagi, H. Löwen and C. Bechinger, *Nature communications*, 2014, **5**, 4829.
15 I. Buttinoni, J. Bialké, F. Kümmel, H. Löwen, C. Bechinger and T. Speck, *Phys. Rev. Lett.*, 2013, **110**, 238301.
16 F. Kümmel, P. Shabestari, C. Lozano, G. Volpe and C. Bechinger, *Soft Matter*, 2015, **11**, 6187–6191.
17 T. Bäuerle, A. Fischer, T. Speck and C. Bechinger, *Nature communications*, 2018, **9**, 3232.
18 R. Golestanian, T. B. Liverpool and A. Ajdari, *Phys. Rev. Lett.*, 2005, **94**, 220801.
19 S. J. Ebbens and J. R. Howse, *Soft Matter*, 2010, **6**, 726–738.
20 M. N. Popescu, S. Dietrich and G. Oshanin, *The Journal of Chemical Physics*, 2009, **130**, 194702.
21 J. L. Anderson, *Annual Review of Fluid Mechanics*, 1989, **21**, 61–99.
22 F. Jülicher and J. Prost, *Phys. Rev. Lett.*, 2009, **103**, 079801.
23 A. Würger, *Phys. Rev. Lett.*, 2015, **115**, 188304.
24 S. Samin and R. van Roij, *Phys. Rev. Lett.*, 2015, **115**, 188305.
25 A. Onuki, *Phase Transition Dynamics*, Cambridge University Press, 2002.
26 H. Ding and P. D. M. Spelt, *Phys. Rev. E*, 2007, **75**, 046708.
27 S. Roy, S. Dietrich and A. Maciołek, *Phys. Rev. E*, 2018, **97**, 042603.
28 S. Roy and A. Maciołek, *Soft Matter*, 2018, **14**, 9326–9335.
29 H. Tanaka and T. Araki, *Phys. Rev. Lett.*, 2000, **85**, 1338–1341.
30 T. Araki and H. Tanaka, *J. Phys.: Condens. Matter*, 2008, **20**, 072101.
31 T. Araki and H. Tanaka, *Phys. Rev. E*, 2006, **73**, 061506.
32 T. Araki and S. Fukai, *Soft Matter*, 2015, **11**, 3470–3479.
33 A. Barbot and T. Araki, *Soft Matter*, 2017, **13**, 5911–5921.
34 H. Tanaka and T. Araki, *Europhys. Lett.*, 2000, **51**, 154–1600.
35 T. Araki and H. Tanaka, *Europhys. Lett.*, 2004, **65**, 214–220.
36 A. Onuki, *Phys. Rev. Lett.*, 2005, **94**, 054501.
37 A. Onuki, *Phys. Rev. E*, 2007, **75**, 036304.
38 R. Teshigawara and A. Onuki, *Europhys. Lett.*, 2008, **84**, 36003.
39 R. Teshigawara and A. Onuki, *Phys. Rev. E*, 2010, **82**, 021603.
40 R. Teshigawara and A. Onuki, *Phys. Rev. E*, 2011, **84**, 041602.
41 A. Pelissetto and E. Vicari, *Phys. Rep.*, 2002, **368**, 549.
42 P. G. de Gennes, *C. R. Acad. Sci. Paris*, 1981, **202**, 701.
43 G. Flöter and S. Dietrich, *Z. Phys. B*, 1995, **97**, 213.
44 A. Hanke and S. Dietrich, *Phys. Rev. E*, 1999, **59**, 5081–5100.
45 S. Yabunaka and A. Onuki, *Phys. Rev. E*, 2017, **96**, 032127.
46 N. O. Young, J. S. Goldstein and M. J. Block, *J. Fluid. Mech.*, 1959, **6**, 350–356.
47 S. Puri, *Journal of Physics: Condensed Matter*, 2005, **17**, R101–R142.
48 H. Tanaka, *Journal of Physics: Condensed Matter*, 2001, **13**, 4637.
49 S. Ebbens, M.-H. Tu, J. R. Howse and R. Golestanian, *Phys. Rev. E*, 2012, **85**, 020401.
50 E. F. Semeraro, R. Dattani and T. Narayanan, *The Journal of Chemical Physics*, 2018, **148**, 014904.

Appendix: Chemical potential

Here we neglect the terms relating to the particles by setting $\psi = 0$. The energy and entropy per solvent molecule are given by

$$e = -\frac{\varepsilon}{2}\phi^2 + \frac{3}{2}k_{\mathrm{B}}T + \frac{K}{2}|\nabla\phi|^2, \tag{A.1}$$

$$s = s_0(\phi) + k_{\mathrm{B}}\ln(v_0/\lambda_T^3), \tag{A.2}$$

where $s_0 = -k_{\mathrm{B}}(a\phi^2/2 + b\phi^4/4)$.

The chemical potential including the gradient term is defined by

$$\mu = -T\left(\frac{\delta\mathscr{S}}{\delta\phi}\right)_e, \tag{A.3}$$

where the energy density e is fixed. From Eq. (A1), this condition leads to

$$-\varepsilon\phi\delta\phi + \frac{3}{2}k_{\mathrm{B}}\delta T + \delta\left(\frac{K}{2}|\nabla\phi|^2\right) = 0. \tag{A.4}$$

The change of the total entropy with respect to infinitesimal changes of ϕ and T is given by

$$\delta\mathscr{S} = \frac{1}{\xi_0^3}\int d\mathbf{r}\left(\frac{\partial s_0}{\partial\phi}\delta\phi + \frac{3}{2}\frac{k_{\mathrm{B}}}{T}\delta T\right). \tag{A.5}$$

With Eq. (A4), Eq. (A5) is rewritten as

$$\begin{aligned}\delta\mathscr{S} &= \frac{1}{\xi_0^3}\int d\mathbf{r}\left\{\frac{\partial s_0}{\partial\phi}\delta\phi + \frac{\varepsilon\phi}{T}\delta\phi - \frac{1}{2}\left(\frac{K}{T}\right)\delta(|\nabla\phi|^2)\right\} \\ &= \frac{1}{\xi_0^3}\int d\mathbf{r}\left\{\frac{\partial s_0}{\partial\phi} + \frac{\varepsilon\phi}{T} + \nabla\cdot\left(\frac{K}{T}\nabla\phi\right)\right\}\delta\phi,\end{aligned} \tag{A.6}$$

where we ignore the effect of the boundary in the integration by parts. Then, we have

$$\left(\frac{\delta\mathscr{S}}{\delta\phi}\right)_e = \frac{\partial s_0}{\partial\phi} + \frac{\varepsilon\phi}{T} + \nabla\cdot\left(\frac{K}{T}\nabla\phi\right) \tag{A.7}$$

Thus, we obtain the chemical potential in an inhomogeneous tem-

perature field from Eq. (A3) as

$$\frac{\mu}{k_{\mathrm{B}}T} = \left(a - \frac{\varepsilon}{k_{\mathrm{B}}T}\right)\phi + b\phi^3 - \nabla\cdot\left(\frac{K}{k_{\mathrm{B}}T}\nabla\phi\right). \qquad \text{(A.8)}$$

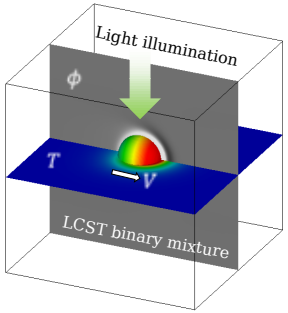

Self-propelled motion of a Janus particle suspended in a binary mixture wi
the lower critical solution temperature under local heating around a cappe
hemisphere